Plasma transport into the duskside magnetopause caused by Kelvin-Helmholtz vortices in response to the northward turning of the interplanetary magnetic field observed by THEMIS

Guang Qing Yan[1], George K. Parks[2], Chun Lin Cai[1], Tao. Chen[1], James P. McFadden[2], Yong Ren[1,3]

[1] State Key Laboratory of Space Weather, National Space Science Center, Chinese Academy of Sciences, Beijing, China, 100190

[2] Space Science Laboratory, University of California, Berkeley, California, USA, CA94720

[3] University of Chinese Academy of Sciences, Beijing, China, 100049

Abstract: A train of Kelvin-Helmholtz (K-H) vortices with plasma transport across the magnetopause has been observed by the Time History of Events and Macroscale Interactions during Substorms (THEMIS) at the duskside of magnetopause. This unique event occurs when the interplanetary magnetic field (IMF) abruptly turns northward, which is the immediate change to facilitate the K-H instability. Two THEMIS spacecraft, TH-A and TH-E, separated by 3 Re, periodically encountered the duskside magnetopause and the low-latitude boundary layer (LLBL) with a period of 2 minutes and tailward propagation of 212 km/s. The rotations in the bulk velocity observation, distorted magnetopause with plasma parameter fluctuations and the magnetic field perturbations, as well as high-velocity low-density feature, indicate the formation of rolled-up K-H vortices at the duskside of magnetopause. The coexistence of magnetosheath ions with magnetospheric ions and enhanced energy flux of hot electrons is identified in the K-H vortices. These transport regions appear more periodic at the upstream spacecraft and more dispersive at the downstream location, indicating a significant transport can occur and evolve during the tailward propagation of the K-H waves. There is still much work to fully understand the Kelvin-Helmholtz mechanism. The observations of direct response to the northward turning of the IMF, the clear evidence of plasma transport within the vortices, involving both ion and electron fluxes can provide additional clues to the K-H mechanism.

Key words: K-H vortices, northward IMF, plasma transport, LLBL

1 Introduction

Kelvin-Helmholtz (K-H) instability can be activated at the interface between different plasma regimes with different velocities, and the perturbations propagate along the direction of the velocity shear as a form of surface wave developing into nonlinear vortices. As shown by Hasegawa (1975), the high density and the magnetic field perpendicular to the velocity shear on either side of the interface facilitate the unstable condition. The fastest K-H instability occurs when the wave vector $\mathbf{k}$ is parallel/antiparallel to the velocity shear and perpendicular to the magnetic field (Southwood, 1979; Manuel & Samson, 1993). This condition favors the low-latitude magnetopause where the velocity shear and the northward magnetospheric magnetic field are available. The magnetic tension stabilizes the shear layer if the magnetic field and the velocity shear are aligned, indicating that the radial IMF does not favor the K-H instability. However, reported observation indicates that K-H waves occur at the high-latitude magnetopause under the dawnward IMF and continues to exist when the IMF turns radial (Hwang et al., 2012). On the other hand, under the radial IMF, K-H instability is found in both simulations (Tang et al., 2013; Adamson et al., 2016) and observations (Farrugia et al., 2014; Grygorov et al., 2016). In some cases, the K-H instability is thought facilitated by a denser boundary layer formed by the dayside magnetic reconnections (Grygorov et al., 2016), by the plasma plume (Walsh et al., 2015), or by the pre-existing denser boundary layer formed by the high-latitude reconnections under the northward IMF (Hasegawa et al., 2009; Nakamura et al. 2017). Theoretically, both northward and southward IMF can favor the K-H instability at the low-latitude magnetopause. In fact, almost all of the previous observations (Chen & Kivelson, 1993; Kivelson & Chen, 1995; Fujimoto et al., 2003; Hasegawa et al., 2004) and simulations (Chen et al., 1997; Farrugia et al., 2003; Miura, 1995; Hashimoto & Fujimoto, 2005) show that the K-H waves occur preferentially under the northward IMF, although linear K-H waves are observed under the southward IMF (Mozer et al., 1994; Kawano et al., 1994). However, under the southward IMF, Cluster has observed nonlinear K-H waves with irregular and turbulent characteristics (Hwang et al., 2011) and THEMIS has observed regular K-H vortices with an induced electric field at the edges (Yan et al., 2014). As reviewed (Johnson et al., 2014; Masson & Nykyri, 2016) recently, observations from many missions such as Cluster, THEMIS, Wind, Geotail etc., as well as simulations greatly enriched our understandings of the K-H instability and the vortices. Based on long term observations, a statistical survey indicates that K-H waves are much more ubiquitous than previously thought (Kavosi & Raeder, 2015), which implies the importance of the solar wind plasma transport into the magnetosphere via the K-H vortices.

In addition to magnetic reconnections at low latitude (Dungey, 1961) and high latitude magnetopause (Song & Russell, 1992), whose nature is a popular research topic (e.g., Dai, 2009; Dai et al., 2017; Dai, 2018), the K-H instability is an important way to transport solar wind into the magnetosphere when reconnections are inactive at the magnetopause. A statistical study of Double Star observations implies the entry of cold ions into the flank magnetopause caused by the K-H vortices that is enhanced by solar wind speed (Yan et al., 2005). However, it is noted that the K-H instability itself cannot lead to plasma transport across the magnetopause (Hasegawa et al., 2004); therefore, certain secondary processes (e.g., Nakamura et al., 2004; Matsumoto & Hoshino, 2004; Chaston et al., 2007) are necessarily coupled with the K-H instability for plasma transport into the magnetosphere via the LLBL. The reconnection of the twisted magnetic field lines inside

the K-H vortex was first found in a simulation (Otto & Fairfield, 2000) and has since been identified in observations (Nykyri et al., 2006; Hasegawa et al., 2009; Li, et al., 2016). The plasma transport into the magnetosphere via such a process in K-H vortices has been quantitatively investigated in a simulation (Nykyri & Otto, 2001). Most recently, energy transport from a K-H wave into a magnetosonic wave was estimated conserving energy in the cross-scale process, and three possible ways were discussed to transfer energy involving shell-like ion distributions, kinetic Alfvén waves, and magnetic reconnection (Moore et al., 2016). Up to now, reports of direct observations of plasma transport in the K-H vortices are only a hand full (e.g., Sckopke et al., 1981; Fujimoto et al., 1998; Hasegawa et al., 2004). Moreover, the microphysical processes for the plasma transport remains unclear, indicating more observations of such a transport process are needed to help us understand the physics. In this work, we present the THEMIS observations of the K-H vortices activated when the IMF abruptly turns northward, without a pre-existing denser boundary layer to facilitate the instability. We show a significant solar wind transport into the magnetosphere occurs and evolves within the vortices.

2 Data and Methods

The THEMIS mission (Angelopoulos, 2008) consists of five identical spacecraft originally orbiting the Earth similar to a string of pearls configuration. In August 2009, TH-B and TH-C were pushed to the vicinity of the lunar orbit, while the other three stayed in the near-Earth orbit with an apogee of approximately 13 Re. The instruments onboard include a flux gate magnetometer (FGM) (Auster et al., 2008) to measure the magnetic field and an electrostatic analyzer (ESA) (McFadden et al., 2008) to measure the electron (6 eV-30 keV) and ion (5 eV-25 keV) fluxes. We used the 3-second averaged FGM and ESA data from TH-A and TH-E to perform the particle analysis, and the 1/16 second averaged FGM data to perform the minimum variance analysis (MVA) (Sonnerup & Cahill, 1967; 1968) to determine the local magnetopause coordinates to find the distortions of the magnetopause. The FGM and ESA data from TH-B located in the dawnside downstream solar wind provide the IMF and solar wind conditions with an estimated time lag of 10 minutes from the subsolar magnetopause to TH-B. Both ion and electron energy spectra with a 3-second resolution were used to diagnose the transport of the magnetosheath and magnetospheric ions. During the interval of interest, there are no data in the top energy channels centered at 25.21 keV for the ion spectrum and 31.76 keV for the electron spectrum, which has not influenced our investigations.

3 Observations and Discussions

During the interval UT 22:20-22:54 on March 28, 2016, TH-A and TH-E were located near the magnetopause (figure 1), while TH-D was located in the inner magnetosphere, far from the magnetopause. TH-B, near the lunar orbit, was immersed in the solar wind at the dawnside downstream of the other two spacecraft. As shown in panel 1 of figure 3, TH-B observed an abrupt turning of the IMF from duskward to northward at UT 22:32, corresponding to UT 22:22, with a time lag of 10 minutes ((10+32.7) Re / (450 km/s)) from the subsolar magnetopause to TH-B. Periodical fluctuations were observed in both the TH-A and TH-E observations (figure 2), from ion density in panel 1, temperature in panel 2, magnetic field in panel 3 and 7, to velocity in panel 4 and 8, especially the alternating appearances of hot and cold ions in the energy-time spectra (panel 5 and 9). The period was approximately 2 minutes (17 peaks within 34 minutes),

and the tailward bulk propagation speed was approximately 212 km/s (3 Re / 90 s). In figure 3, the rotational characteristics were identified in the periodical fluctuations in V_l, V_m and V_n with phase differences between them. The magnetic field deviations in panels 3 and 5 indicated the perturbations of the magnetic field along with the deformation of the magnetopause. The alternating appearances of the two different plasmas imply the multiple periodic encounters of the magnetopause and the LLBL, which is one of the typical characteristics of K-H vortices.

In this event, the IMF is strongly northward, and the observed magnetic field doesn't change much, so it could be difficult to identify the magnetopause. We selected the four intervals of UT 22:24:00-22:24:40, UT 22:32:40-22:33:10, UT 22:35:50-22:36:10, UT 22:28:50-22:39:20, marked by the black arrows, when the TH-A ion spectrum showed the magnetosheath feature. During the four intervals, TH-A observed magnetosheath cold ions without magnetospheric hot ions (green regions at top of panel 5, figure 2). The absence of hot ions indicated that the spacecraft had crossed the magnetopause into the magnetosheath, where the outbound and inbound crossings of the magnetopause can be identified in the ion spectrum. At each pair of traversals, the local magnetopause coordinates LMN were calculated by using MVA (Sonnerup & Cahill, 1967; 1968). The details and results of MVA calculations are listed in table 1. In the calculations of MVA, relative large ratios of the second to third eigenvalues r_{23} =$\varepsilon_2/\varepsilon_3$ means better reliability of determination of local coordinates (e.g. Sergeev et. al., 2006). In the MVA results, it can be seen that 4 of 8 eigenvalue ratios are larger than 3, indicating the good reliability of the MVA method at their corresponding crossings, even though the magnetic field doesn't change strongly. At least at these traversals, the magnetopause was deformed to the nonlinear vortices. The calculated normal direction N as well as the tangential direction M of the local magnetopause is used to identify the distorted magnetopause. In each panel of figure 4, the normal and tangential directions M-N at the outbound and inbound magnetopause are plotted in the equatorial plane, compared with the average M-N of the magnetopause. The average magnetopause in dotted line, as well as the average M-N directions, is calculated from the model (Shue, 1998), and the dotted line is also approximately the trajectory of the spacecraft TH-A, which is moving at a relatively slow speed of about 2 km/s at the apogee. The distorted magnetopause is plotted in black line, perpendicular to N and parallel to M at outbound and inbound. The deviations of the M-N directions from the averaged magnetopause illustrate the magnetopause distortions formed by the K-H vortices. Such distortions of the magnetopause qualitatively explain the periodically alternating encounters of magnetosphere-like and magnetosheath-like plasmas. The plasma rotation is also illustrated by the red circle with arrow, consistent with the observations in panel 4 of figure 2.

The high-speed and low-density feature is one of the fundamental characteristics of rolled-up vortices (Nakamura et al., 2004; Takagi et al., 2006), and has been used to identify vortices in a single spacecraft measurements (e.g., Hasegawa et al., 2006; Hwang et. al., 2011, Grygorov et al., 2016). We estimated the magnetosheath velocity by averaging the TH-A measurements during the four magnetosheath intervals mentioned above, with the magnetosheath velocity of about 134 km/s. Figure 5 shows the V_m-N_i plot, in which the blue lines mark the high-speed and low-density region. V_m is the tailward velocity, the M component of the measured velocity expressed in the averaged magnetopause coordinates LMN. Substantial data points are distributed in blue box in figure 5, and the high-speed low-density feature can be seen in the Ni-Vm plot. Hence then, the rotations of the plasma flows, the perturbations of the magnetic field, the high-velocity and low

163   density feature, and the distortions of the magnetopause support the formation of rolled-up K-H
164   vortices. It is worth noting that the first peak arrived as soon as the IMF turned northward at UT
165   22:22, which can facilitate the K-H instability.

166   Before and after the UT 22:22-22:52 interval, the magnetospheric hot ions dominated in panel 5
167   of figure 2, mainly in the 3-25 keV range with an energy flux of 10^6 eV/(cm^2-s-sr-eV), and the
168   magnetospheric hot electrons dominated in panel 6, mainly in the 0.5-25 keV range with an
169   energy flux of over 10^7 eV/(cm^2-s-sr-eV). The typical temperatures of magnetospheric hot ions
170   and electrons were about 4 keV and 0.3 keV, respectively. On the other hand, during the UT
171   22:22-22:52 interval, the repeating magnetosheath cold ions in panel 5 were primarily observed
172   between 0.1-3 keV with an energy flux of over 10^6 eV/(cm^2-s-sr-eV), and the cold electrons in
173   panel 6 were observed between 10-500 eV, with an energy flux of over 10^7 eV/(cm^2-s-sr-eV). The
174   typical temperatures of magnetosheath cold ions and electrons were about 0.2 keV and 0.05 keV,
175   respectively. Embedded in the plasmas of the two different origins, the coexisting hot and cold
176   ions overlapped. Taking the mass ratio of protons to electrons into account, the gyro-radius of the
177   electrons is only 1/42 of protons with the same energy and the same magnetic field, estimated to
178   be approximately 2 km. We understand the ion transport as the coexistence of magnetosheath and
179   magnetospheric ions in the observations, characterized by the substantial cold ions in the steady
180   background of the hot plasma. For the proton's gyro-radius of approximately 80-100 km at the
181   magnetopause, the coexistence of the hot and cold ions in the spectrum is not sufficient to
182   diagnose the mixture of the two components. Thus, we used the observed hot electrons as an
183   additional indicator of the magnetosphere region because of their relatively smaller gyro-radius.
184   Hence, the criteria to identify the mixture/transport are described such that the cold ions of 0.1-3
185   keV can be observed with an energy flux over 10^5 eV /(cm^2-s-sr-eV) in the hot ions background,
186   with an energy flux over 10^6 eV /(cm^2-s-sr-eV), as well as a substantial enhancement in the energy
187   flux of the hot electrons of 0.5-5 keV. Based on such criteria, the ion mixture/transport intervals
188   were diagnosed from both TH-A and TH-E, marked by the green bars at the bottom of panel 6 and
189   the black bars at the bottom of panel 10 in figure 2. The transport regions in the TH-A
190   observations (green bars) were distributed at the edges of the vortices and appeared to be more
191   periodic, while those in the TH-E observations (black bars) were more dispersive.
192   The coexistence of hot and cold ions is one direct feature of the solar wind transport into
193   the magnetosphere, as clearly displayed in Geotail observations by Fujimoto et. al. (1998) and
194   in Cluster observations by Hasegawa et. al. (2004). In this event, the coexistence of hot and
195   cold ions was firstly noted near the periodically oscillating magnetopause. Furthermore, we
196   used the enhancement of hot electron flux as an indicator of the magnetosphere, and set up the
197   more critical criteria to diagnose the coexistence, and hence to display the transport regions,
198   as marked by the green bars at the bottom of panel 6 and black bars at the bottom of panel 10
199   in figure 2. The evidence of the plasma transport is clearly shown in this event. By comparing
200   the green bars and the black bars, it can be found that the transport regions in TH-A
201   observations appears more periodic but those in TH-E observations more dispersed. The
202   difference between the features of transport regions at upstream TH-A and downstream TH-E
203   implies the plasma transport significantly occurred and evolved during the tailward
204   propagation, along with the collapse of the vortices, leading to a kind of turbulence state, as
205   illustrated in previous simulations (Nakamura et al., 2004; Matsumoto & Hoshino, 2004).
206   TH-A observed very clearly periodic motions of magnetopause during the 34 minutes

except UT 22:46-22:50, TH-E observed relatively much more dispersed spectrum during the interval but 5 clear oscillations appeared again during UT 22:40-22:48. However, it seems true that, on the whole, the spectrum observed at TH-E is much more turbulent than the periodic spectrum at TH-A. Such an evolution implies the collapse of the vortices and the evolution leading to turbulence state. In previous simulations (Nakamura et al., 2004; Matsumoto & Hoshino, 2004), the vortices collapse and cause transport of the solar wind into magnetosphere, after that, new vortices may be generated at the recovered magnetopause. The 5 oscillations during UT 22:40-22:48 at downstream TH-E can by explained as newly formed vortices. As mentioned above, the first K-H wave, as well as the transport regions arrived at the upstream TH-A as soon as the IMF abruptly turned northward. The K-H vortices were evidently activated as a response to the abrupt northward turning of the IMF, which was the direct change to facilitate the K-H instability immediately.

Previously, both electron and ion distributions were used to diagnose the region of observation (Chen et al., 1993). While diagnosing the transport regions in this event, the typical plasma features in different regions were selected for comparisons (figure 6), as illustrated by the energy flux distributions of both ions (blue line) and electrons (red line). In panels 1, both the ion and electron fluxes show single-peak at the low energy, indicating the components of cold and dense magnetosheath plasma. In panel 2, the ion flux shows a double-peak, which means the coexistence of the magnetosheath cold ions and magnetospheric hot ions. The relatively smaller peak/enhancement in the electron flux show that the magnetospheric hot electrons are detected, but the cold electrons dominate, implying the spacecraft is located in magnetosheath but very close to the magnetospause, a coexistence region. In panel 3, both the ion and electron fluxes show double-peak. The double-peak of the ion flux indicates coexistence of the magnetosheath cold ions and magnetospheric hot ions. For the electron flux, the peak at the high energy indicates that more magnetospheric hot electrons are detected, implying that the spacecraft is located in magnetosphere, another example of coexistence region. In panel 4, both ion and electron fluxes show single-peak at the high energy, indicating the components of hot and tenuous magnetospheric plasma. It should be noted that the ion flux plots (blue lines in each panel) should be lower in the tail, but show no such decrease tails in part because the data were absent at the high energy channels. The typical regions shown correspond to the magnetosheah, the energetic particle streaming layer, the LLBL, and the magnetosphere (Sibeck, 1991).

4 Summary

We analyzed observations from TH-A and TH-E that periodically encountered the LLBL; the K-H vortices were identified by the rotation features in the bulk velocity, magnetic field deviations, the high-speed low-density features and the distortions of the magnetopause deduced by MVA, which indicate the generation of K-H vortices. The K-H vortices started as soon as the IMF turned northward abruptly, which is the direct change to facilitate the instability immediately. By considering the enhancement of the hot electrons as an indicator of the magnetosphere region, the ion transport regions were shown that significant plasma transport can occur during the tailward propagation from TH-A to TH-E. Typical plasma features were observed in different regions. These new observations characterized by the direct response to the northward turning of the IMF, the clear evidence of plasma transport involving both ion and electron fluxes, can complement existing observations and enhance our understanding of the plasma transport processes in K-H

250 vortices.

Data Availability

252 The data for this paper are available at the Coordinated Data Analysis Web of NASA's Goddard
253 Flight Center (http://cdaweb.gsfc.nasa.gov/istp_public/).

Authors Contribution

255 G. Q. Y. designed the idea and carried out the investigations, prepared the manuscript with
256 contributions from all co-authors. G. K. P, C. L. C, and T. C. offered the valuable scientific
257 discussions and helped to improve the manuscript. J. P. M. ensured the data and gave valuable
258 suggestions. R. Y. prepared some of the figures.

Competing Interests

260 The Authors declare that they have no conflict of interest.

Acknowledgements

262 This work was supported by the Strategic Pioneer Program on Space Science, Chinese
263 Academy of Sciences, Grant No. XDA15052500, XDA15350201, and XDA17010301, and by the
264 National Natural Science Foundation of China, Grant No. 41574161, 41731070, 41574159 and
265 41004074. The authors are grateful to NASA's Goddard Flight Center and the associated
266 instrument teams for supplying the data. The Authors thank Professor Chi Wang and Professor Lei
267 Dai for valuable scientific discussions. The authors also express their thanks for the support from
268 the Specialized Research Fund for State Key Laboratories and the CAS-NSSC-135 project. Part of
269 the work was done during G. Q. Yan's visit at UC Berkeley, who cordially appreciates the
270 assistance from Professor Forrest S. Mozer.

271

References

273 Adamson, E., Nykyri, K., and Otto, A.: The Kevin-Helmholtz instability under Parker-Spiral
274 interplanetary Magnetic Field conditions at the magnetospheric flanks, Adv. Space Res., 58,
275 218-230, 2016.
276 Angelopoulos, V.: The THEMIS mission, Space Sci. Rev., 141, 5–34,
277 doi:10.1007/s11214-008-9336-1, 2008.
278 Angelopoulos, V., The ARTEMIS mission, Space Sci. Rev., 165, 3–25,
279 doi:10.1007/s11214-010-9687-2, 2011.
280 Auster, U., Glassmeier, K. H., Magnes, W., Aydogar, O., Baumjohann, W., Constaninescu, D.,
281 Fischer, D., Fornicon, K. H., Georgescu, E., Harvey, P., Hillenmaier, O., Kroth, R., Ludlam, M.,
282 Narita, Y., Nakamura, R., Okrafca, K., Plaschke, F., Richter, I., Schwartzl, H., Stoll, B.,
283 Vanavanoglou, A., Wiedemann, M.: The THEMIS fluxgate magnetometer, Space Sci. Rev., 141,
284 235–264, doi:10.1007/s11214-008-9365-9, 2008.
285 Chaston, C. C., Wilber, M., Mozer, F. S., Fujimoto, M., Goldstein, M. L., Acuna, M., Rème, H.,
286 and Fazakerley, A.: Mode conversion and anomalous transport in Kelvin-Helmholtz vortices and
287 kinetic Alfven waves at the Earth's magnetopause, Phys. Rev. Lett., 99, 175004, Doi:

10.1103/PhysRevLett.99.175004, 2007.

Chen, Q., Otto, A., and Lee, L. C.: Tearing instability, Kelvin-Helmholtz instability, and magnetic reconnection, J. Geophys. Res., 102(A1), 151-161, 1997.

Chen, S. H., and Kivelson, M. G.: On nonsinusoidal waves at the magnetopause, Geophys. Res. Lett., 20, 2699-2702, 1993.

Chen, S.-H., Kivelson, M. G., Gosling, J. T., Walker, R. J., and Lazarus, A. J.: Anomalous aspects of magnetosheath flow and of the shape and oscillations of the magnetopause during an interval of strongly northward interplanetary magnetic field, J. Geophys., 98, 5727-5742, 1993.

Dai, L.: Collisionless Magnetic Reconnection via Alfven Eigenmodes, Phys. Rev. Lett., 102, 245003, doi:https://doi.org/10.1103/PhysRevLett.102.245003, 2009.

Dai, L., Wang, C., Zhang, Y., Lavraud, B., Burch, J., Pollock, C., and Torbert, R. B.: Kinetic Alfvén wave explanation of the Hall fields in magnetic reconnection, Geophys. Res. Lett., 44, 634–640, doi:10.1002/2016GL071044, 2017.

Dai, L.: Structures of Hall Fields in Asymmetric Magnetic Reconnections, J. Geophys. Res. Space Physics, 123(9), 7332-7341, doi: https://doi.org/10.1029/2018JA025251, 2009.

Dungey, J. W.: Interplanetary magnetic field and auroral zones, Phys. Rev. Lett. 6(2), 47-48, 1961.

Farrugia, C. J., F. T. Gratton, G. Gnavi, R. B. Torbert, L. B. Wilson, A vortical dawn flank boundary layer for near-radial IMF: Wind observations on 24 October 2001, J. Geophys. Res. Space Physics, 119, 4572-4590, doi: 10.1002/2013JA019578, 2014.

Fujimoto, M., Terasawa, T., Mukai, T., Saito, Y., Yamamoto, T., and Kokubun, S.: Plasma entry from the flanks of the near-Earth magnetotail: Geotail observations, J. Geophys.Res. 103(A3), 4391-4408, 1998.

Fujimoto M., Tonooka, T., and Mukai, T.: Vortex-like fluctuations in the magnetotail flanks and their possible roles in plasma transport in the Earth's Low-Latitude Boundary Layer, Geophys. Monogr. Ser., vol. 133. Edited byNewell, P. T., and Onsager, T., p. 241, AGU., Washington D. C., 2003.

Grygorov, K., Němeček, Z., Šafránková, J., Přech, L., Pi, G., Shue, J.-H.: Kelvin-Helmholtz wave at the subsolar magnetopause boundary layer under radial IMF. J. Geophys., Res. Space Physics, 121, 9863-9879, doi: 10.1002/2016JA023068, 2016.

Hasegawa, A.: Plasma instabilities and Non-linear effects, Springer-Verlag, New York, 1975.

Hasegawa, H., Fujimoto, M., Phan, T.-D., Rème, H., Balogh, A., Dunlop, M. W., Hashimoto, C., and TanDokoro, R.: Transport of solar wind into Earth's magnetosphere through rolled-up Kelvin-Helmholtz vortices. Nature, 430, 755-758, doi:10.1038/nature02799, 2004.

Hasegawa, H., Fujimoto, M., Takagi, K., Saito, Y., Mukai, T., and Rème, H.: Single-spacecraft detection of rolled-up Kelvin-Helmholtz vortices at the flank magnetopause. J. Geophys. Res., 111, A09203, doi:10.1029/2006JA011728, 2006.

Hasegawa, H., Retinò, A., Vaivads, A., Khotyaintsev, Y., André, M., Nakamura, T. K. M., Teh, W. –L., Sonnerup, B. U. Ö., Schwartz, S. J., Seki, Y., Fujimoto, M., Saito, Y., Rème, H., and Canu, P.: Kelvin-Helmholtz waves at the Earth's magnetopause: Multiscale development and associated reconnection, J. Geophys. Res., 114, A12207, doi:10.1029/2009JA014042, 2009.

Hashimoto, C., and Fujimoto, M.: Kelvin-Helmholtz instability in an unstable layer of finite thickness, Adv. Space Res., 37, 527-531, 2005.

Hwang, K.-J, Kuznetsova, M. M., Sahraoui, F., Goldstein, M. L., Lee, E., and Parks, G. K.: Kelvin-Helmholtz waves under southward interplanetary magnetic field, J. Geophys. Res., 116,

A08210, doi:10.1029/2011JA016596, 2011.

Hwang, K.-J., Goldstein, M. L., Kuznetsova, M. M., Wang, Y., Vinas, A. F., and Sibeck, D. G.: The first in situ observation of Kelvin-Helmholtz waves at high-latitude magnetopause during stongly dawnward interplanetary magnetic field conditions, J. Geophys. Res., 117, A08233, doi: 10.1029/2011JA017256, 2012.

Johnson, J. R., Wing, S., Delamere, P. A.: Kelvin Helmholtz Instability in Planetary Magnetospheres, Space Sci. Rev., 184, 1-31, doi: 10.1007.s11214-014-0085-z, 2014.

Kavosi, S. and Raeder, J.: Ubiquity of Kelvin-Helmholtz waves at Earth's magnetopause. Nat. Commun., 6:7019, doi:10.1038/ncomms8019, 2015

Kawano, H., Kokubun, S., Yamamoto, Y., Tsuruda, K., Hayakawa, H., Nakamura, M., Okada, T., Matsuoka, A., and Nishida, A.: Magnetopause characteristics during a four-hour interval of multiple crossings observed with GEOTAIL, Geophys. Res. Lett., 21, 2895-2898, 1994.

Kivelson, M. G., and Chen, S. H.: The magnetopause: Surface waves and instabilities and their possible dynamic consequences, in Physics of the Magnetopause, Geophys. Monogr. Ser., vol. 90. Edited by Song, P., Sonnerup, B. O. Ü., and Thomsen, M. F., p. 257, AGU., Washington D. C., 1995.

Li, W. Y., André, M., Khotyaintsev, Y. V., Vaivads, A., Graham, D. B., Toledo-Redondo, S., and Strangeway, R. J.: Kinetic evidence of magnetic reconnection due to Kelvin-Helmholtz waves. Geophys. Res. Lett., 43, 5635-5643, doi: 10.1002/2016GL069192, 2016.

Manuel, J. R., and Samson, J. C.: The Spatial Development of the Low-latitude Boundary Layer. J. Geophys. Res., 98(A10), 17367-17385, 1993.

Masson, A., and Nykyri, K.: Kelvin-Helmholtz Instability: Lessons Learned and Ways Forward. 214, 71-89, doi:10.1007/s11214-018-0505-6, 2018.

Matsumoto Y., and Hoshino, M.: Onset of turbulence induced by a Kelvin-Helmholtz vortex. Geophys. Res. Lett., 31, L02807, doi: 10.1029/2003GL018195, 2004.

McFadden, J. P., Carlson, C. W., Larson, D., Ludlam, M., Abiad, R., Elliott, B., Turin, P., Marckwordt, M., and Angelopoulos, V.: The THEMIS ESA plasma instrument and in-flight calibration. Space Sci. Rev., 141, 277–302, doi:10.1007/s11214-008-9440-2, 2008.

Miura, A.: Dependence of the magnetopause Kelvin-Helmholtz instability on the orientation of the magnetosheath magnetic field. Geophys. Res. Lett., 22, 2993-2996, 1995.

Moore, T. W., Nykyri, K., Dimmock, A. P.: Cross scale energy transport in space plasmas. Nat. Phys., 12, 1164-1169, doi: 10.1038/nphys3869, 2016.

Mozer, F. S., Hayakawa, H., Kokubun, S., Nakamura, M., Okada, T., Yamamoto, T., and Tsuruda, K.: The morningside low-latitude boundary layer as determined from electric field and magnetic field measurements on Geotail, Geophys. Res. Lett., 21, 2983-2886, 1994.

Nakamura, T. K. M., Hayashi, D., and Fujimoto, M.: Decay of MHD-Scale Kevin-Helmholtz Vortices Mediated by Parasitic Electron Dynamics. Phys. Rev Lett., 92(14), 145001, doi: 10.1103/PhysRevLett.92.14501, 2004.

Nakamura, T. K. M., Eriksson, S., Hasegawa, H., Zenitani, S., Li, W. Y., Genestreti, K. J., Nakamura, R., and Daughton, W.: Mass and Energy Transfer across the Earth's Magnetopause Caused by Vortex-Induced Reconnection, J. Geophys. Res.: Space Physics, 122, 11505-11522, doi: 10.1002/2017JA024346, 2017.

Nykyri, K., and Otto, A.: Plasma transport at the magnetospheric boundary due to reconnection in Kelvin-Helmholtz vortices, Geophys. Res. Lett., 28, 3565-3568, 2001.

376   Nykyri, K., Otto, A., Lavraud, B., Mouikis, C., Kistler, L. M., Balogh, A., and Rème, H.:
377   Cluster observations of reconnection due to the Kelvin-Helmholtz instability at the dawnside
378   magnetosphere flank, Ann. Geophys., 24, 2619-2643, 2006.

379   Otto, A, and Fairfield, D. H.: Kelvin-Helmholtz instability at the magnetotail boundary: MHD
380   simulation and comparison with Geotail observations, J. Geophys. Res., 105(A9), 21175-21190,
381   2000.

382   Sergeeve, V. A., Sormakov, D. A., Apatenkov, S. V., Baumjohann, W., Nakamura, R., Runov, A.
383   V., Mukai, T., and Nagai, T.: Survey of large-amplitude flapping motions in the midtail current
384   sheet, Ann. Geophys., 24, 2015-2024, 2006.

385   Shue, J.-H., Song, P., Russell, C. T, Steinberg, J. T., Chao, J. K., Zastenker, G., Vaisberg, O. L.,
386   Kokubun, S., Singer, H. J., Detman, T. R., and Kawano, H.: Magnetopause location under extreme
387   solar wind conditions, J. Geophys. Res., 103, 17691-17700, 1998.

388   Sibeck, D. G.: Transient event in the Outer magnetosphere: boundary waves or flux transfer
389   event? J. Geophys. Res., 97(A4), 4009-4026, 1992.

390   Sckopke, N., Paschmann, G., Haerendel, G., Sonnerup, B. U. Ö., Bame, S. J., Forbes, T. G.,
391   Hones Jr, E. W., andRussell, C. T.: Structure of the Low- Latitude Boundary Layer, J. Geophys.
392   Res., 86(A4), 2099-2110, 1981.

393   Sonnerup, B. U. Ö., and Cahill, L. J.: Magnetopause structure and attitude from Explorer 12
394   observations, J. Geophys. Res., 72, 171-183, 1967.

395   Sonnerup, B. U. Ö., and Cahill, L. J.: Explorer 12 observations of the magnetopause current
396   layer, J. Geophys. Res., 73, 1757-1770, 1968.

397   Song P., and Russell, C. T.: Model of the formation of the low-latitude-boundary-layer for
398   strongly northward interplanetary magnetic field, J. Geophys. Res., 97(A2), 1411-1420, doi,
399   10.1029/91JA02377, 1992.

400   Southwood, D. J.: Magnetopause Kelvin-Helmholtz instability, in Magnetosphere Boundary
401   Layers, edited by Battrick, B., and Mort, J., pp. 357-364, European Space Agency Scientific and
402   Technical Publications Branch, Noordwijk, The Netherlands, 1979.

403   Tang, B. B., Wang, C., and Li, W. Y.: The magnetosphere under the radial interplanetary
404   magnetic field: A numerical study, J. Geophys., Res. Space Physics, 118, 7674-7682, doi:
405   10.1002/2013JA019155, 2013.

406   Walsh, B. M., Thomas, E. G., Hwang, K. -H., Baker, J. B. H., Ruohoniemi, J. M., Bonnell, J. W.:
407   Dense plasma and Kelvin-Helmholtz waves at Earth's dayside magnetopause, J. Geophys. Res.:
408   Space Physics, 120, 5560-5573, doi: 10. 1002/2015JA021014, 2015.

409   Yan, G. Q., Shen, C., Liu, Z. X., Rème, H., Carr, C. M., and Zhang, T. L.: A Statistical Study
410   on Correlations between Plasma Sheet and Solar Wind Based on DSP Explorations, Ann.
411   Geophys., 23, 2961-2966, 2005.

412   Yan, G. Q., Mozer, F. S., Shen, C., Chen, T., Parks, G. K., Cai, C. L., McFadden, J. P.:
413   Kelvin-Helmholtz Vortices observed by THEMIS at the duskside of the magnetopause under
414   southward IMF. Geophys. Res. Lett., 41, 4427-4434, doi:10.1002/2014GL060589, 2014.

420 Figures and Captions
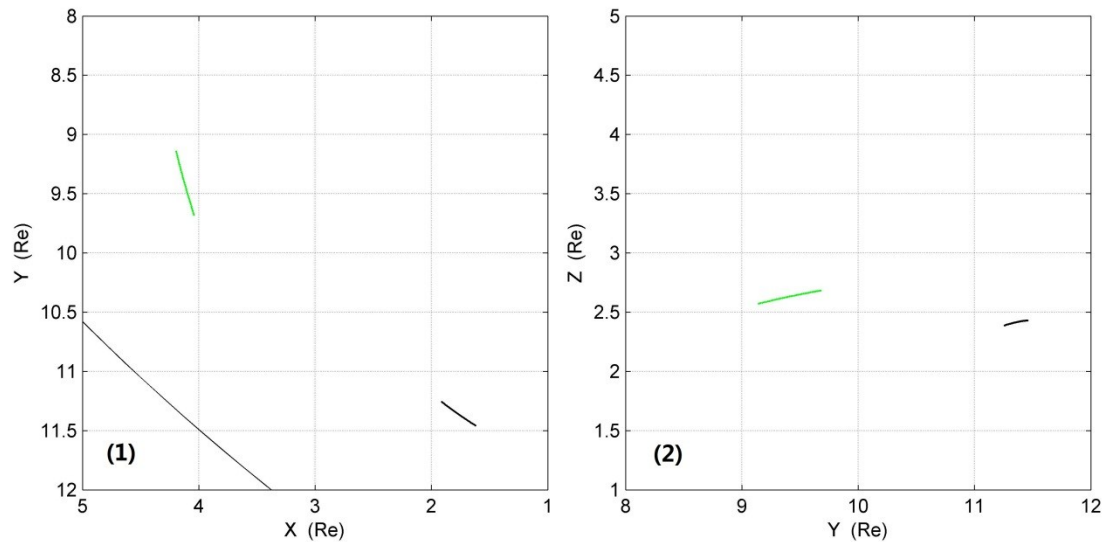
421
422 Figure 1. The orbits and positions of TH-A (green) and TH-E (black) during the interval of interest UT 22:20 ~ UT
423 22:54. The position data are expressed in GSM coordinates.
424
425
426
427
428
429
430
431
432
433
434
435
436
437
438
439
440
441
442
443

444
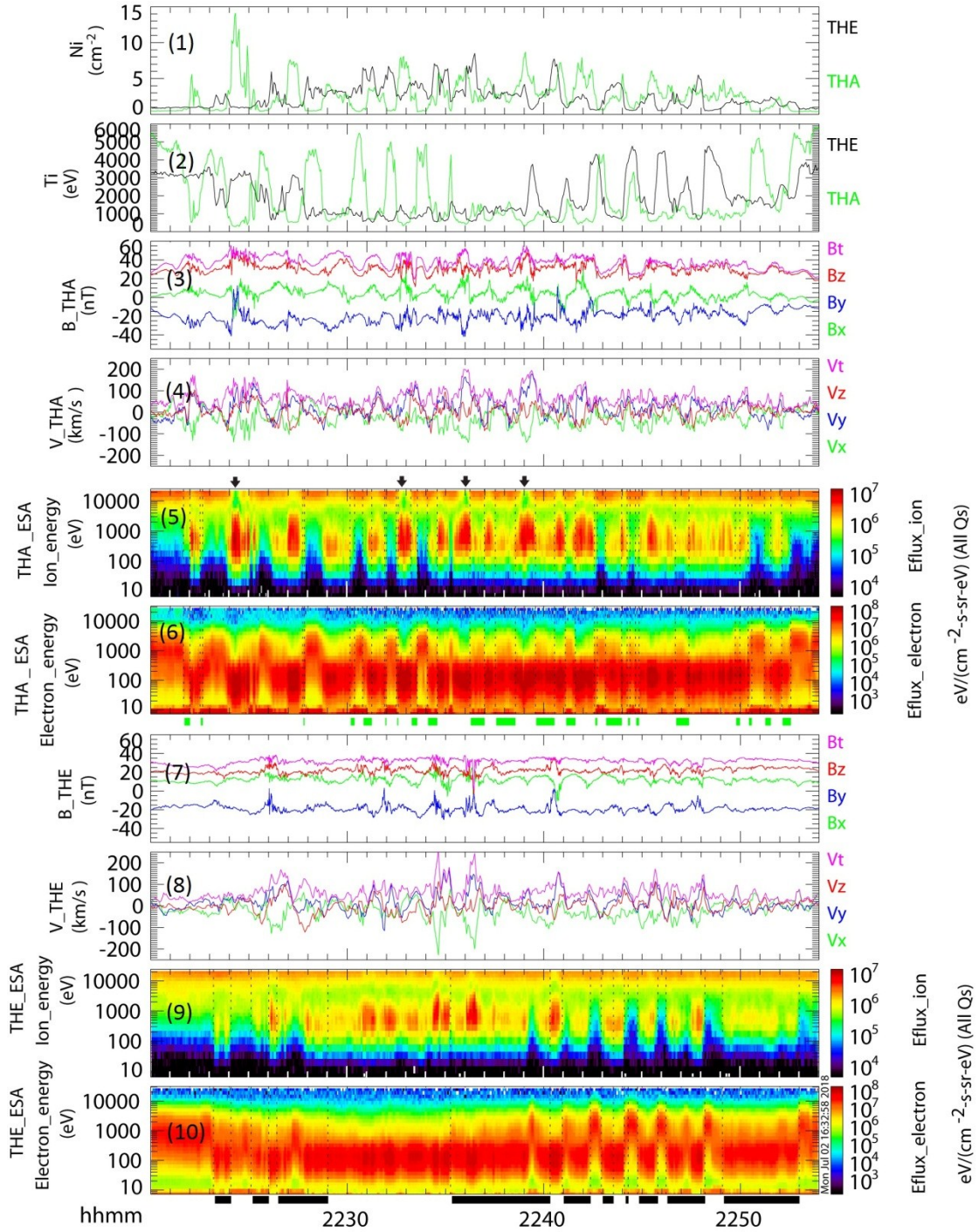
445 Figure 2. Fluctuations in the plasma parameters and the ion and electron energy-time spectra. Panel 1 is the ion

446 densities from TH-A as a green line and from TH-E as a black line; panel 2 is the ion temperatures from TH-A as a

447 green line and from TH-E as a black line; panels 3 and 4 are the magnetic field vectors and the ion bulk velocity

448 vectors from TH-A, respectively; panels 5 and 6 are the ion and electron energy-time spectra from TH-A,

449 respectively; panels 7 and 8 are the magnetic field vectors and the ion bulk velocity vectors from TH-E,

450 respectively; panels 9 and 10 are the ion and electron energy-time spectra from TH-E, respectively. Vectors are all

451 expressed in GSM coordinates. The four black arrows mark on top of panel 5 the TH-A intervals in the

452 magnetosheath. The green bars on the bottom of panel 5 and the black bars on the bottom of panel 9 mark the

453 transport regions in TH-A and TH-E observations, respectively, identified based on the criteria dictated in the text.

454
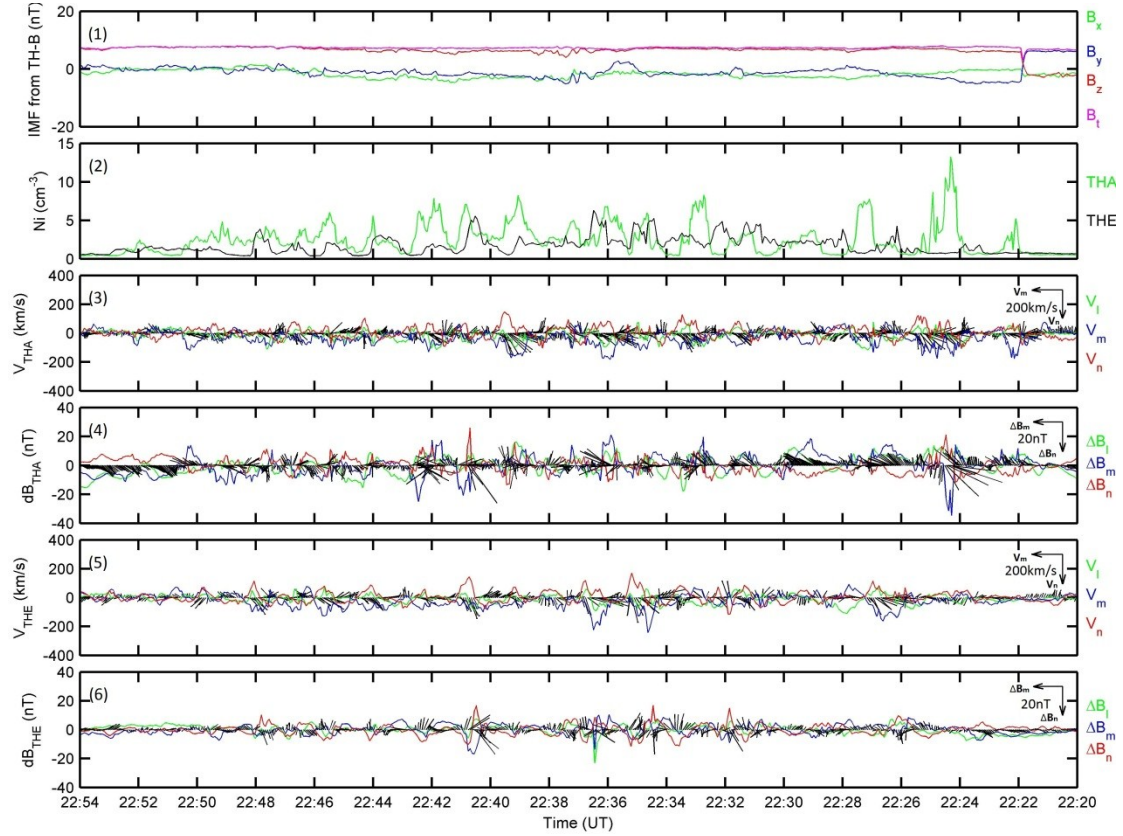
455 Figure 3. The observed plasma rotations and perturbations of the magnetic field because of the formation of K-H

456 vortices. Panel 1 is the IMF monitored by TH-B near the lunar orbit, with a time lag of 10 minutes from subsolar

457 magnetopause to TH-B; panel 2 are the ion densities from TH-A in green and from TH-E in black; panels 3 and 5

458 are the ion bulk velocities from TH-A and TH-E, respectively, expressed in averaged local magnetopause

459 coordinates LMN, deduced from the magnetopause model (Shue et al., 1998); panels 4 and 6 are the magnetic field

460 perturbations, $\Delta \boldsymbol{B} = \boldsymbol{B} - \boldsymbol{B}_{\text{mean}}$, from TH-A and TH-E respectively, expressed in LMN. Note that the time begins from

461 the right and passes to the left, so that the *M* component orients leftward and N component orients downward in

462 the plots.

463

464

465

466

467

468

469

470

471

472

473

474

475

476

477

478   Table 1. Results of MVA analysis at the four magnetosheath encounters of TH-A. The ratio of the second to third

479   eigenvalues $r_{23}=\varepsilon_2/\varepsilon_3$ are shown in the right column.

Num	Time interval	L	M	N	$r_{23} =\varepsilon_2/\varepsilon_3$
1	22:23:50-22:24:12	0.0637	0.4374	0.8970	4.56
		-0.3955	-0.8141	0.4251	
		0.9162	-0.3819	0.1212	
2	22:24:20-22:25:15	0.0646	-0.3877	-0.9195	5.27
		-0.2602	0.8830	-0.3906	
		0.9634	0.2645	-0.0438	
3	22:32:30-22:32:52	0.0017	0.8349	0.5504	1.82
		-0.6860	-0.3995	0.6081	
		0.7276	-0.3786	0.5721	
4	22:32:52-22:33:14	-0.0561	-0.3946	-0.9171	2.25
		0.3303	0.8595	-0.3900	
		0.9422	-0.3248	0.0821	
5	22:35:35-22:36:00	0.2636	0.1004	0.9594	3.34
		-0.4912	-0.8420	0.2231	
		0.8302	-0.5301	-0.1726	
6	22:36:07-22:36:20	-0.0102	0.3363	-0.9417	2.77
		0.0117	0.9417	0.3362	
		0.9999	-0.0076	-0.0135	
7	22:38:41-22:39:05	0.2307	0.0363	0.9724	3.42
		-0.4125	-0.9014	0.1315	
		0.8813	-0.4314	-0.1930	
8	22:39:05-22:40:30	-0.0574	-0.5073	-0.8599	1.07
		-0.7802	-0.5145	0.3556	
		0.6229	-0.6913	0.3662	

480

481

482

483

484

485
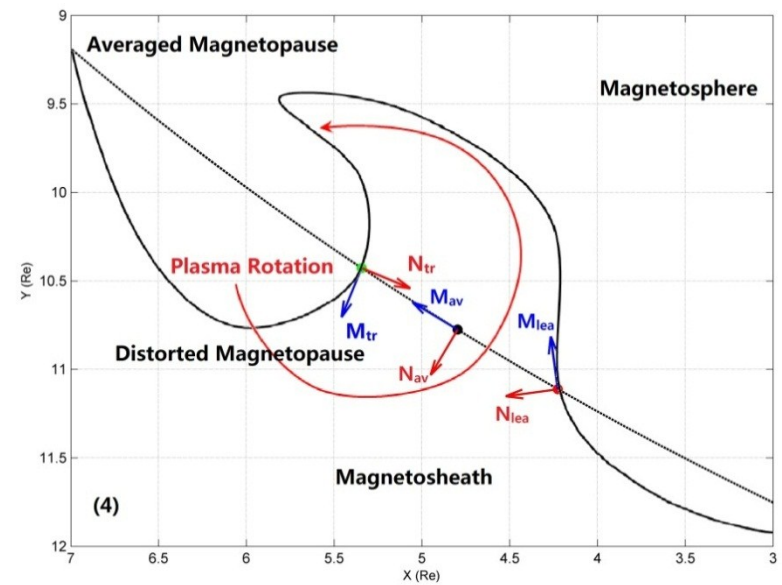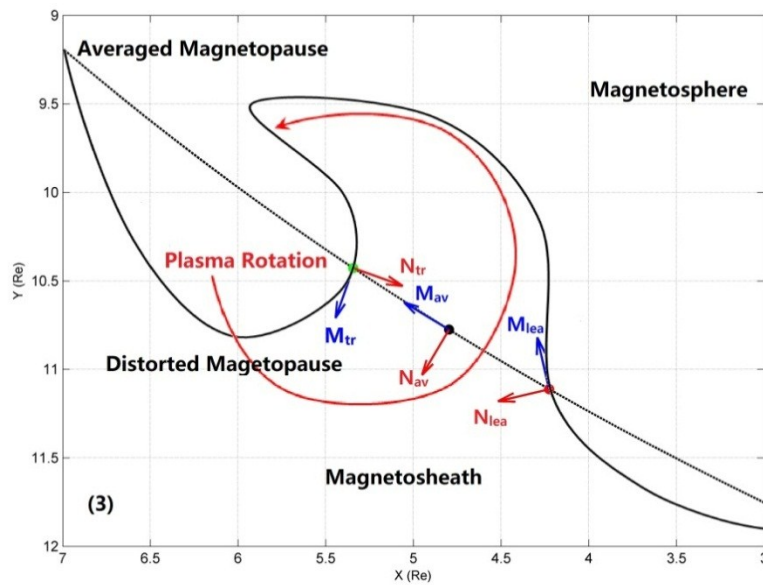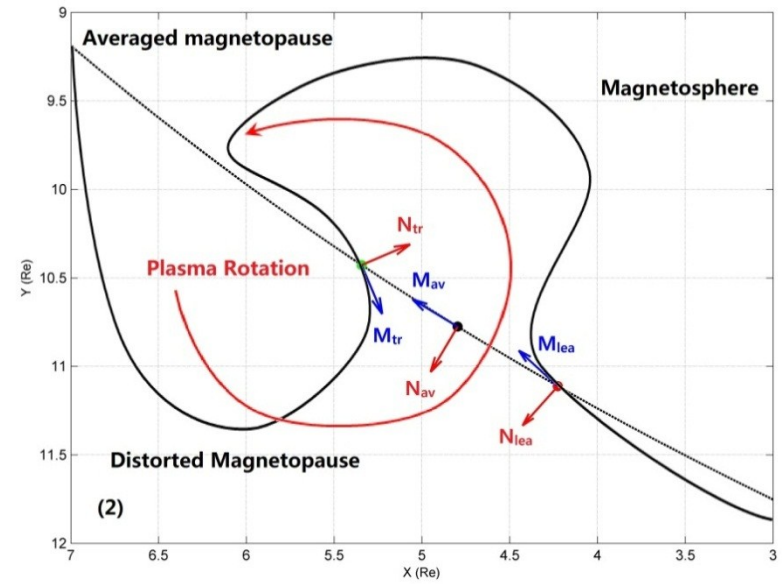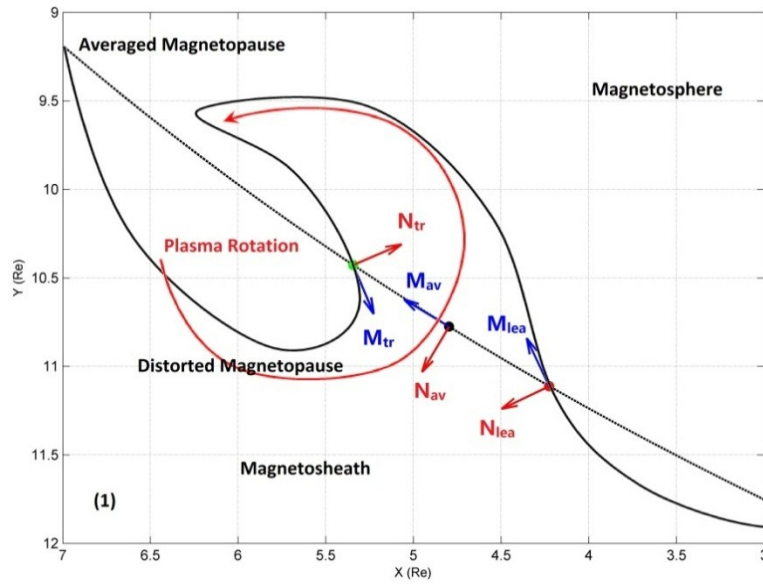
Figure 4. The magnetopause distortions formed by the K-H vortices deduced by the MVA. The average magnetopause (dashed lines), approximated to the spacecraft trajectory, was calculated from the magnetopause model (Shue et al., 1998). Traversal pair at UT 22:24 in panel 1: M_{lea}=(0.4374, -0.8141, -0.3819) and N_{lea}=(0.8970, 0.4251, 0.1212) at the outbound crossing; M_{tr}=(-0.3877, 0.8830, 0.2645) and N_{tr}=(-0.9195, -0.3906, -0.0438) at the inbound crossing. Traversal pair at UT 22:32 in panel 2: M_{lea}=(0.8349, -0.3995, -0.3786) and N_{lea}=(0.5504, 0.6081, 0.5721) at the outbound crossing; M_{tr}=(-0.3946, 0.8595, -0.3248) and N_{tr}=(-0.9171, -0.3900, 0.0821) at the inbound crossing. Traversal pair at UT 22:36 in panel 3: M_{lea}=(0.1004, -0.8420, -0.5301) and N_{lea}=(0.9594, 0.2231, -0.1726) at the outbound crossing; M_{tr}=(0.3363, 0.9417, -0.0076) and N_{tr}=(-0.9417, 0.3362, -0.0135) at the inbound crossing. Traversal pair at UT 22:39 in panel 4: M_{lea}=(0.0363, -0.9014, -0.4314) and N_{lea}=(0.9724, 0.1315, -0.1930) at the outbound crossing; M_{tr}=(-0.5073, -0.5145, -0.6913) and N_{tr}=(-0.8599, 0.3556, 0.3662) at the inbound crossing.
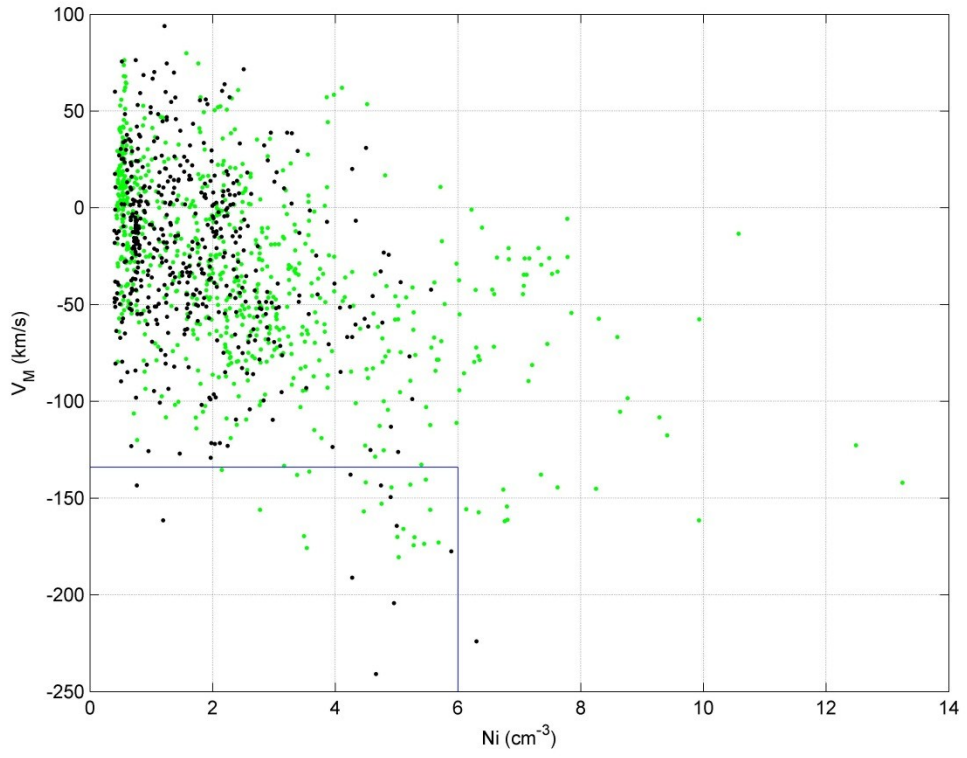
Figure 5. The observed velocity along the tailward direction versus the ion density. Green dots are from TH-A

observations and black dots from TH-E observations. The blue lines mark the high-speed and low density region

possibly caused by the acceleration of the rotation.
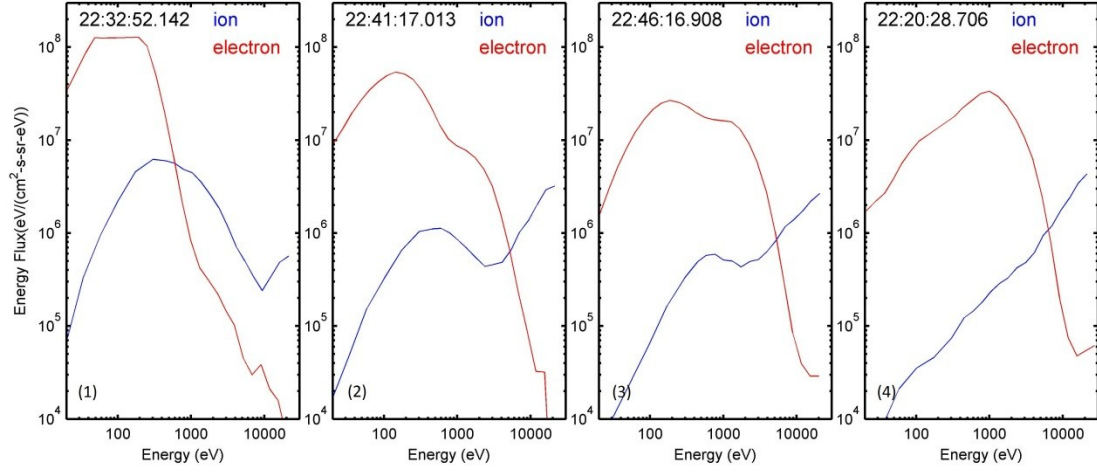
Figure 6. Typical portraits of the energy-time spectra of plasmas in different regions. Panel 1 is the magnetosheath observed by TH-A at 22:32:52.142; panel 2 is co-existence region I observed by TH-A at 22:41:17.013; panel 3 is co-existence region II observed by TH-E at 22:46:16.908; panel 4 is the magnetosphere observed by TH-A at 22:20:28.706.